Cold-crystallization in liquid crystalline poly(*p*-hydroxybenzoic acid-*co*-ethylene terephthalate)

P. G. Hedmark, P.-E. Werner*, M. Westdahl* and U. W. Gedde†
Department of Polymer Technology, The Royal Institute of Technology, S-100 44 Stockholm, Sweden
(Received 19 February 1988; revised 10 November 1988; accepted 9 March 1989)

Quenched samples of thermotropic liquid crystalline poly(*p*-hydroxybenzoic acid (HBA)-*co*-ethylene terephthalate (ETP)) with a HBA/ETP molar ratio of 0.6:0.4 have been annealed at temperatures between 401.3 K and 451.5 K. Thermal analysis (differential scanning calorimetry, d.s.c.) and wide-angle X-ray scattering indicate that two types of crystallization occur at these temperatures: comparatively large (> 10 nm) HBA-rich crystals of a high melting point are formed most probably due to a transesterification reaction-induced crystallization; thin, about 3 nm thick, HBA-rich crystals are formed by 'normal' cold-crystallization. Avrami analysis of the latter process recorded by d.s.c. yields Avrami exponent values in the range 0.2–0.4 which is consistent with the occurrence of a highly restricted one-dimensional crystal growth. This can be explained on the basis of the limited length of the crystallizable units and on the rigid-rod character of the molecules in the nematic mesophase.

(Keywords: thermotropic liquid crystalline copolyester; poly(*p*-hydroxybenzoic acid-*co*-ethylene terephthalate); annealing; cold-crystallization; transesterification reaction; d.s.c.; wide-angle X-ray scattering)

INTRODUCTION

Thermotropic liquid crystalline poly(*p*-hydroxybenzoic acid-*co*-ethylene terephthalate) with a *p*-hydroxybenzoic acid/ethylene terephthalate (HBA/ETP) molar ratio of 0.6:0.4 is a two-phase system with a 1–2 μm spheres enriched in ETP surrounded by a matrix phase enriched in HBA[1–4]. It is clear from these data that the two comonomers are not uniformly distributed in the molecules. Both *intra-* and *inter*molecular heterogeneity are characteristics of this polymer. The ETP- and HBA-rich phases are associated with two different glass transitions (T_g), in this paper referred to as the lower and the upper T_g occurring at, respectively, 330–340 and 430–450 K (refs. 1–3).

The lower T_g which is associated with the ETP-rich phase, has all the characteristics of a 'normal' glass transition. Dielectric studies[2] indicate that the ETP-rich phase is constrained by the surrounding HBA-rich mesophase: the dielectric α relaxation (corresponding to the lower T_g) is symmetrically broadened with a symmetric width parameter of 0.2–0.3 which is about the same as is obtained for semicrystalline PETP. Differential scanning calorimetry (d.s.c.) and mechanical measurements of samples annealed at temperatures between 310 K and 330 K indicate the occurrence of physical ageing[5].

Earlier X-ray work[6,7] has indicated the presence of some HBA crystallinity in oriented samples of this copolymer. Menczel and Wunderlich[3] observed by d.s.c. a small endothermal peak at 520 K, which they assigned to HBA crystallinity.

The initial aim with the present work was to study possible physical ageing occurring in the HBA-rich glassy liquid crystalline phase associated with the upper T_g. However, the samples crystallized when annealed at temperatures near the upper T_g. X-ray diffraction and thermal analysis data presented in this paper provide information about both the crystallization kinetics and the crystal structure formed.

EXPERIMENTAL

The polymer studied is a copolyester based on HBA and ETP, with a HBA/ETP molar ratio of 0.6:0.4. The synthesis and structure of this polymer are described elsewhere[1,8].

Annealing procedure. Samples weighing approximately 20 mg taken from quenched films were annealed for different periods of time (60–6×10^6 s) at six temperatures between 401.3 K and 451.5 K. Annealing for 60–6000 s was carried out in a temperature-calibrated Perkin-Elmer DSC-2. Annealing for 6×10^4–1×10^6 s was carried out in a temperature-calibrated hot stage.

Differential scanning calorimetry was performed on the annealed samples in a Perker-Elmer DSC-2, which was energy- and temperature-calibrated according to standard procedures. The annealed samples were heated from 300 to 550 K at a rate of 10 K min^{-1} while the differential heat flow was recorded.

Wide-angle X-ray scattering (WAXS) was performed on 150 μm samples both directly after rapid cooling in water (quenching) and after annealing of the quenched samples at 410, 429 and 440 K for, respectively, 1.39×10^6, 5.76×10^4 and 1.1×10^5 s. A sample which had been annealed at 440 K for 1.1×10^5 s and cooled to 300 K

* Department of Structural Chemistry, University of Stockholm, S106 91 Stockholm, Sweden
† To whom correspondence should be addressed

0032-3861/89/112068-06$03.00

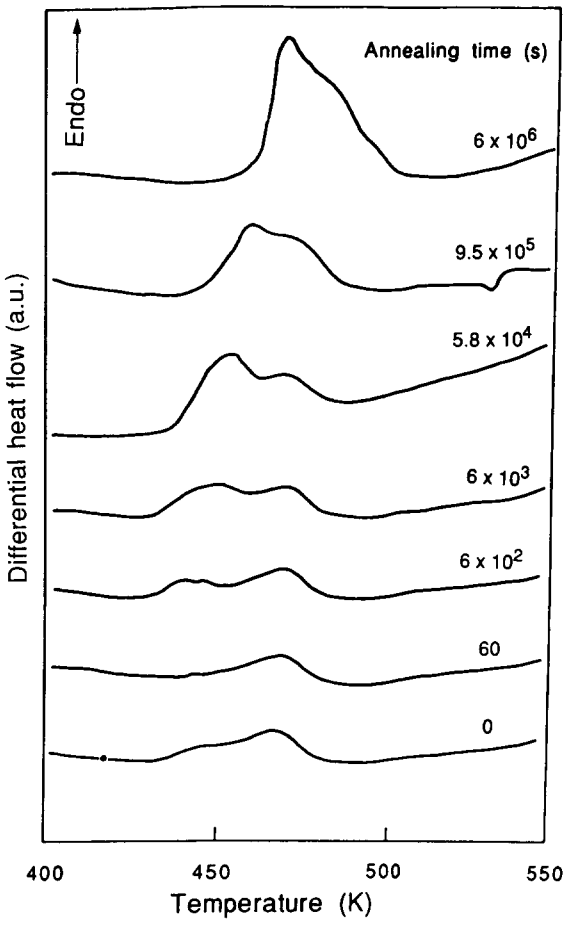

Figure 1 D.s.c. thermograms of samples annealed at 429 K for different periods of time

was heated to 508 K, kept at that temperature for 10 min and then quenched in ice water prior to the X-ray analysis. The analysis was performed in a focusing Guinier-Hägg camera with transmission geometry. Strictly monochromatized CuKα_1 radiation with $\lambda = 0.15406$ nm and single-coated films were used. The accuracy of the measured Bragg angles was tested by photographs taken with silicon added as internal theta standard. The use of an internal standard reduces zero-point errors to a negligible value, corrects for film shrinkage and makes it possible to correct for geometrical errors in the camera. The films were evaluated by a computer-controlled single-beam microdensitometer[9].

RESULTS AND DISCUSSION

Thermograms for a series of annealed samples (T_a = 429.5 K) are shown in *Figure 1*. The original quenched sample displays a small second-order transition (glass transition) at about 430 K and a broad first-order transition around 470 K. This does not change by annealing. Another first-order transition peak (TX) clearly develops on annealing. On prolonged annealing this peak becomes more intensive and is shifted to higher temperatures.

Figures 2 and *3* present a summary of the calorimetric data obtained for TX. The peak temperature increases in a non-linear manner (by 20–30 K over the experimental range) in the plot shown in *Figure 2*. The TX peak is always located at a temperature higher than the corresponding annealing temperature (*Figure 2*). The peak temperature of short-time annealed samples is 5–10 K higher than the corresponding annealing temperature (*Figure 2*). The enthalpy change involved with the TX transition, denoted ΔH, increases in a non-linear manner with the logarithm of the annealing time (*Figure 3*). The increase in ΔH is more rapid at the higher temperatures (see inset in *Figure 3*). It is not possible to establish any 'equilibrium' ΔH values at the different temperatures since the curves shown in *Figure 3* display no levelling-off tendencies.

The calorimetric data strongly suggest that crystal-

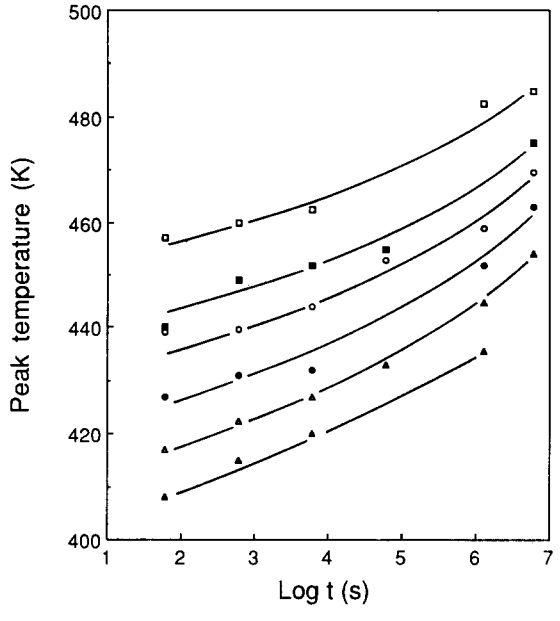

Figure 2 Peak temperature *versus* the logarithm of the annealing time. Annealing temperature (T_a): 401.3 K (▲); 409.5 K (△); 419.5 K (●): 429.5 (○); 440 K (■), 451.5 K (□)

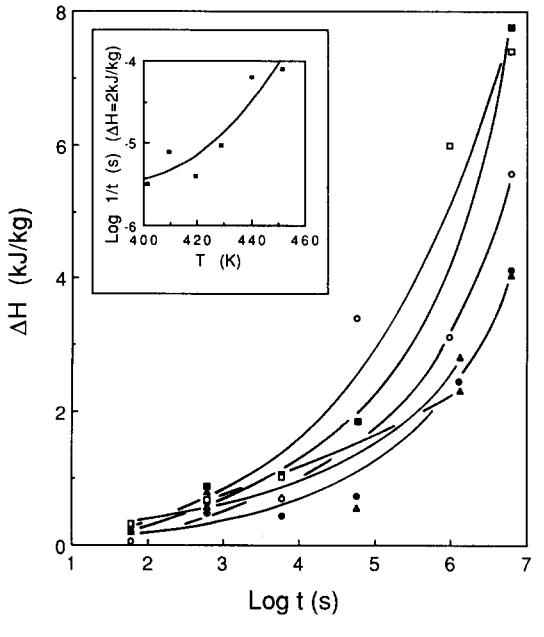

Figure 3 Integral heat of melting of TX peak (ΔH) *versus* the logarithmic of the annealing time for samples annealed at different temperatures (T_a): 401.3 K (▲); 409.5 K (△); 419.5 K (●); 429.5 K (○); 440 K (■); 451.5 K (□). The inset shows the logarithm of the reciprocal time for development of $\Delta H = 2\,\mathrm{kJ\,kg^{-1}}$ as a function of annealing temperature

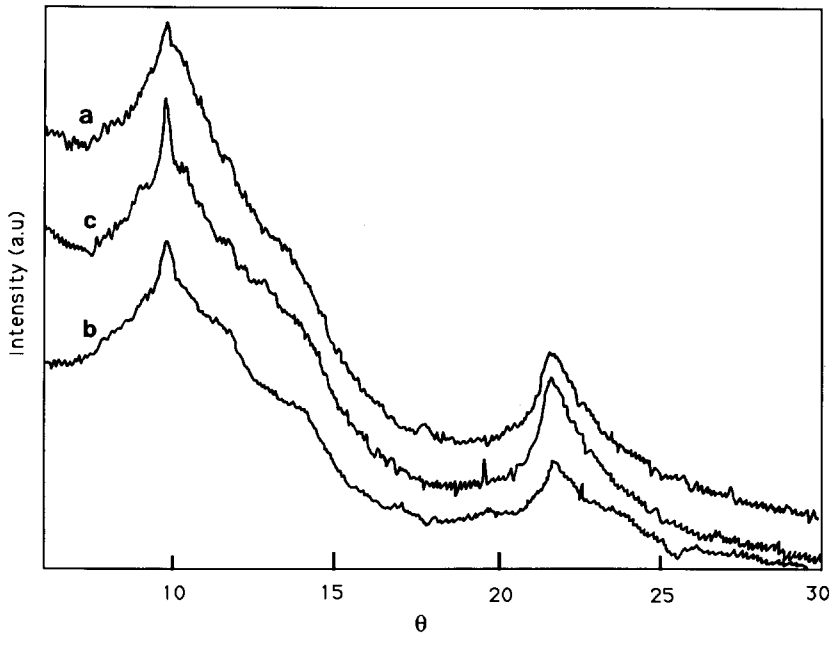

Figure 4 WAXS pattern from samples with different thermal histories: (a) quenched; (b) annealed at 410 K for 1.39×10^6 s; (c) annealed at 429 K for 5.76×10^4 s

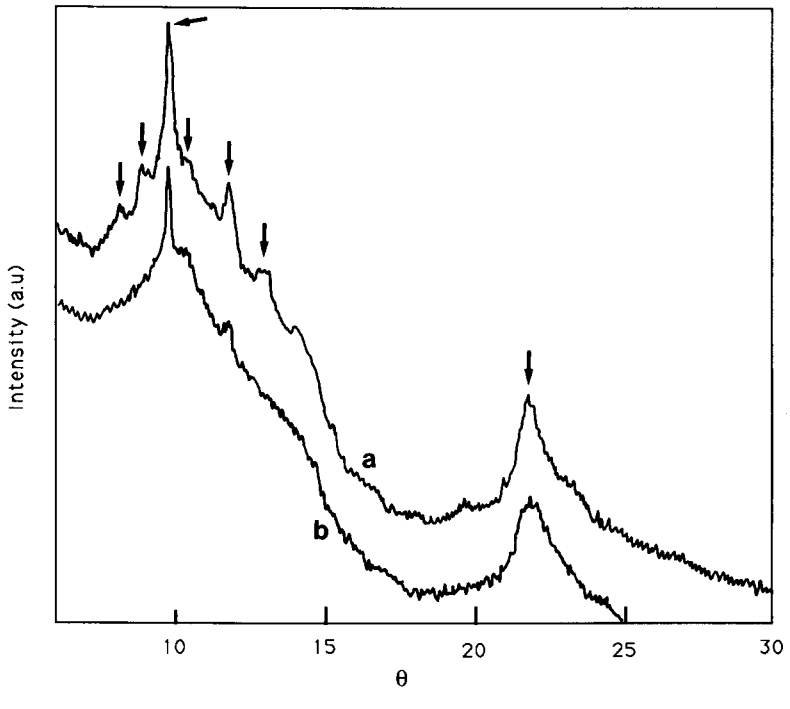

Figure 5 WAXS pattern from samples of the following thermal histories: (a) annealed at 440 K for 1.1×10^5 s; (b) annealed at 440 K for 1.1×10^5 s, cooled to 300 K, heated to 508 K, kept at 508 K for 10 min and quenched in ice water (*q–a* sample). Arrows indicate reflections used for determination of unit cell

lization occurs on annealing. X-ray data (*Figures 4* and *5*) are however, necessary to establish the nature of the crystallization. The quenched sample displays two distinct but broad maxima (*d*-spacings: 0.453 and 0.207 nm) and a shoulder between (*d*-spacing: 0.34 nm). The annealed samples have developed seven sharper crystalline Bragg reflections (*Figures 4* and *5*). The line corresponding to the *d*-spacing value of 0.453 nm ($\theta = 9.8°$) is very strong.

Table 1 presents a comparison of the *d*-spacings obtained from the diffractograms shown in *Figures 4* and *5* and literature data on PETP and PHBA. There is a strong similarity between the copolymer samples presently studied and PHBA. Particularly convincing is the similarity in *d*-spacing values of the most intensive line recorded for PHBA (*d*-spacing: 0.450 nm) and the major diffraction peak recorded in the copolymer samples (*d*-spacing: 0.453 nm).

From the sample annealed at 440 K (*Figure 5*) displaying seven lines, an orthorhombic unit cell with the following dimension was obtained: $a = 0.828$ nm; $b =$

Table 1 Comparison of d spacings (in nm) from annealed samples of PEPT, PHBA and P(HBA-*co*-ETP) 0.6:0.4

PETP[a]	PHBA[b]	P(HBA-*co*-ETP) 0.6:0.4[c]
0.537	0.557[s]	0.544[w]
0.4985	0.510[m]	0.494[m]
0.4085	0.450[vs]	0.453[vs]
0.3869	0.424[m]	0.424[m]
0.3718	0.372[vs]	0.378[m]
0.3408	0.358[s]	0.344[w]
0.1937	0.208[s]	0.207[s]

[a] Data from reference 10
[b] Data on fibrous PHBA from reference 4
[c] Data for sample annealed at 440 K for 1.1×10^5 s. The full diffraction pattern is shown in *Figure 5*
The diffraction peaks are classified in intensities as follows: w = weak; m = medium; s = strong; vs = very strong.

0.606 nm; $c = 1.177$ nm; volume = 0.591 nm^3. The unit cell was found by the trial-and-error indexing program TREOR[11]. As only seven lines are observed, statistical significant figure of merit tests for the powder indexing cannot be made. The average deviation between observed and calculated Bragg angles is only 0.013° and the proposed cell is small and of high symmetry. Furthermore, high quality diffractograms of annealed oriented PHBA reveal an orthorhombic unit cell with similar dimensions: $a = 0.752$ nm; $b = 0.558$ nm; $c = 1.251$ nm, volume = 0.525 nm^3 (ref. 4). The anticipated small and imperfect crystals in the samples of this study broaden the diffraction peaks and increase the uncertainty of the d-spacing values. The discrepancy in the above unit cell data is within the error of the experiment taking the aforementioned factors into consideration.

The question which arises at this point is if the PHBA crystals observed by WAXS are responsible for the TX melting. This was controlled by heating a sample which had been annealed at 440 K for 1.1×10^5 to 508 K and then quenched in ice water. This sample is referred to as *q–a* sample. The *q–a* sample displayed no TX melting as recorded by d.s.c. but surprisingly it exhibited the seven Bragg reflections which were found in the diffractograms of the annealed samples (*Figure 5*). The intensities of the Bragg reflections are however lower in the *q–a* sample than in the corresponding annealed sample (*Figure 5*). It should be noted that the diffractograms shown in *Figure 5* are from samples of the same thickness which were irradiated by the same dose of X-ray. The area under the major diffraction peak ($d = 0.453$ nm) is significantly smaller in the *q–a* sample, only 30–40% of that of the annealed sample. The crystalline material which is molten by the heating to 508 K and which does not recrystallize during the subsequent quenching clearly exhibits the diffraction pattern of PHBA (cf. diffractograms a and b in *Figure 5*). The crystalline material associated with the TX melting peak is thus enriched in HBA. Furthermore, the major diffraction peak ($d = 0.453$ nm) is significantly sharper in the *q–a* sample than in the annealed sample (*Figure 5*) indicating a larger average crystal size in the *q–a* sample. Thus the TX melting should be associated with thinner crystals. This is further substantiated by considering the crystal thickness associated with the TX peak melting as determined from a Thomson–Gibbs equation plot (*Figure 6*). The calculated crystal thickness as obtained from the peak temperature of the TX transition is about 3 nm assuming pure PHBA crystallinity and 2.5 nm assuming pure PETP crystallinity.

The width of the X-ray diffraction peaks reveals information about the crystal size and the paracrystalline distortion[15]. However, the number of Bragg reflections is not sufficient for an analysis by which crystal size and paracrystalline distortion can be separately determined.

By applying the familiar Scherrer equation:

$$L_{hkl} = K\lambda/[\beta_0 \cos\theta] \quad (1)$$

where K is a constant near unity, λ is the wavelength of the X-ray radiation, β_0 is the breadth in radians at the half-maximum intensity of the pure reflection profile, and θ is the diffraction angle, a crystal size normal to (1 1 0) of 30 nm is obtained for the annealed sample shown in *Figure 5*. For other directions normal to (0 2 4), (2 2 2) and (2 0 0) a crystal size of well over 10 nm is obtained for this sample. The size of the crystal normal to (1 1 0) is about 60 nm for the *q–a* sample, i.e. twice the value obtained for the annealed sample. Thus, the Bragg reflections from the annealed sample seem to be a 'composite' of the sharper lines associated with the thicker crystals displayed by the *q–a* sample and the broader reflections associated with the thin crystals responsible for the TX melting.

The following hypothesis, consistent with *both* d.s.c. and X-ray data, is proposed: two types of crystals are formed during annealing at temperatures between 400 K and 450 K.

(1) Comparatively large HBA-rich crystals with a melting point higher than 508 K. These crystals which typically constitute 30–40% of the crystalline material in the long-time annealed samples are not responsible for the so-called TX melting. The major difference in temperature between melting and annealing seems anomalous. However, Lenz *et al.*[16] have reported that a transesterification reaction occurs in this copolymer. It is therefore suggested that relatively long sequences of HBA segments are formed during annealing. These blocks may then crystallize (*reaction-induced crystallization*).

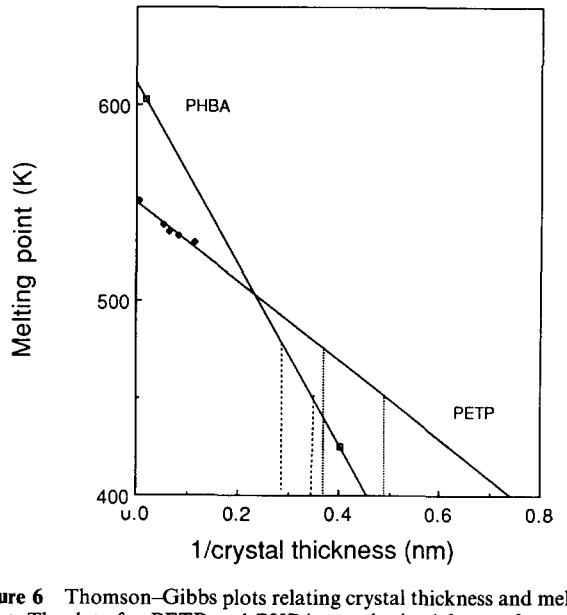

Figure 6 Thomson–Gibbs plots relating crystal thickness and melting point. The data for PETP and PHBA are obtained from reference 12 and references 13 and 14, respectively. Melting point data relating to the TX peak is shown

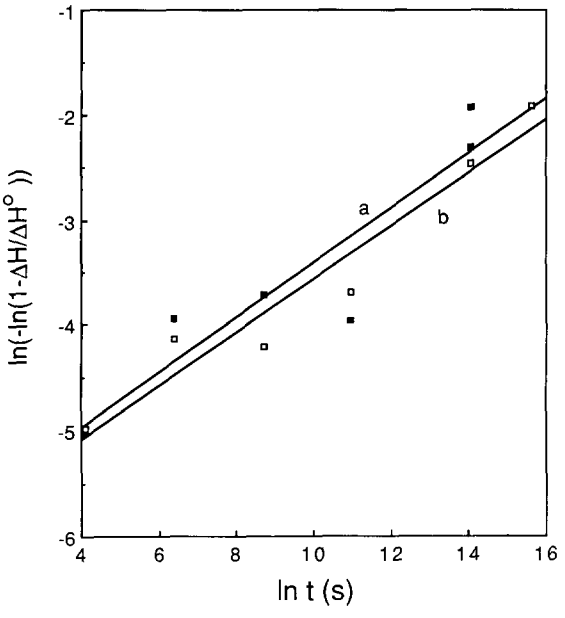

Figure 7 Avrami plots based on d.s.c. data obtained at $T_a = 429.5$ K (a, □) and 451.5 K (b, ■)

Table 2 Avrami exponent (n) data

Annealing temperature (K)	Avrami exponent (n)
401.3	0.21
409.5	0.24
419.5	0.25
429.6	0.36
440.0	0.27
451.5	0.29

(2) Thin (3 nm) crystals associated with the TX melting. WAXS indicates that they are rich in HBA and that they constitute the major part of the crystalline material in the long-time annealed samples. Furthermore, the calorimetric data, i.e. the development of the TX peak, shows the features typical of a crystallization process occurring during the annealing.

Standard Avrami analysis according to:

$$\ln[-\ln(1-\Delta H/\Delta H^\circ)] = \ln K + n \ln t \qquad (2)$$

where ΔH° is the heat of fusion for a 100% crystalline sample, K is a constant and n is the Avrami exponent was performed on the crystallization kinetic data (TX peak) shown in *Figure 3*. *Figure 7* presents two typical linear Avrami plots. The slope of the lines in the Avrami diagram, i.e. the Avrami exponent (n) is not particularly sensitive to the choice of ΔH° value. The Avrami exponent values presented in *Table 2* are all based on $\Delta H^\circ = 30\,\mathrm{kJ\,kg^{-1}}$. This value is estimated on the basis of data in the literature on crystal–nematic melt phase transitions of polyesters[17–19]. The values of the Avrami exponent presented in *Table 2* are all very low, typically about 0.3.

The exponent in the Avrami equation was derived long ago for a number of different nucleation types and crystal growth types and geometries. An excellent review of this topic is given by Wunderlich[20]. The low value obtained for the Avrami exponent requires a highly restricted low dimensional crystal growth, preferably one-dimensional (fibrillar) growth. The restrictions on the crystal growth may be of two different types: decrease in crystal growth rate with time; limiting size of the crystals. Both these factors tend to depress the Avrami exponent. *Table 3* presents a summary of Avrami exponents as derived for a few nucleation and crystal growth characteristics.

There are a number of arguments in favour of restricted, one-dimensional crystallization in the considered polymer. Firstly, small crystal size is expected from the fact that the sample is of low crystallinity and that it is a copolymer. Secondly, the nematic mesophase, which consists of rod-like molecules which are relatively free to move in the chain direction, will be immobilized by the crystallization. The transport of the crystallizable sequences will be strongly hindered by the crystals (physical crosslinks) and the stiff character of the chains. The rate of crystallization is thus expected to decrease significantly with time. This may be a general characteristic of liquid crystalline polymers. Conventional flexible-chain polymers, on the other hand, have chain flexibility sufficient to uncouple the different crystallizable sequences. Lastly, the crystals should be uncorrelated, i.e. crystallization is not a sequential-type of process as in spherulitic crystallization of flexible-chain polymers. The latter give rise to an Avrami exponent of 3–4 (ref. 20).

CONCLUSIONS

When heated, quenched samples of thermotropic liquid crystalline poly(*p*-hydroxybenzoic acid-*co*-ethylene terephthalate) with HBA/ETP molar ratio of 0.6:0.4 annealed at temperatures near the upper T_g (401.3–451.5 K) display a first-order endothermal transition at temperatures 5–40 K higher than the annealing temperature. X-ray diffraction shows that HBA-rich crystals are formed during annealing. Furthermore, by comparison of the data from WAXS and d.s.c., mainly focusing on the crystal size, it can be concluded that two types of crystallization occur on annealing. The first involves the formation of comparatively large (>10 nm) HBA-rich crystals of high melting point probably by a transesterification reaction-induced crystallization. The second which can be characterized as 'normal' cold-crystallization give rise to low-melting, thin (3 nm) HBA-rich crystals. Avrami analysis of d.s.c. data on the latter process yields Avrami exponent values of about 0.3 which is consistent with a highly restricted one-dimensional crystal growth. Crystallization is expected to be restricted both in terms of final crystal size and transport of crystallizable units. The low chain flexibility of the rigid-rod molecules will hinder molecules physically crosslinked in crystals from slipping past other molecules for the transport of the crystallizable sequences.

Table 3 Avrami exponent (n) predictions

Nucleation	Crystal growth	n
Athermal	One-dimensional (fibrillar), constant growth rate, unlimited size	1
Athermal	One-dimensional (fibrillar), diffusion controlled growth, unlimited size	0.5
Athermal	One-dimensional (fibrillar), diffusion controlled growth, limited size	<0.5
Thermal	One-dimensional (fibrillar), constant growth rate, unlimited size	2
Athermal	Two-dimensional (circular disc), constant growth rate, unlimited size	2

ACKNOWLEDGEMENTS

The reported study has been sponsored by the National Swedish Board for Technical Development (STU), grant no. 85-3593 and the Swedish Natural Science Research Council (NFR), grant no. K-RT 1910-100. The authors wish to thank Dr W. J. Jackson Jr., Tennessee Eastman Co., USA for providing the polymer studied.

REFERENCES

1 Hedmark, P. G., Jansson, J.-F., Hult, A., Lindberg, H. and Gedde, U. W. *J. Appl. Polym. Sci.* 1987, **34**, 743
2 Gedde, U. W., Buerger, D. and Boyd, R. H. *Macromolecules* 1987, **20**, 988
3 Menczel, J. and Wunderlich, B. *J. Polym. Sci., Polym. Phys. Edn.* 1980, **18**, 1433
4 Blackwell, J., Lieser, G. and Gutierrez, G. A. *Macromolecules* 1983, **16**, 1418
5 Hedmark, P. G., Dick, R. W. R. and Gedde, U. W. Unpublished data
6 Wissbrun, K. F. *Br. Polym. J.* 1980, **12**, 163
7 Acierno, D., La Mantia, F. P., Polizzotti, G., Ciferri, A. and Valenti, B. *Macromolecules* 1982, **15**, 1455
8 Jackson, Jr, W.J. and Kuhfuss, H. G. *J. Polym. Sci., Polym. Chem. Edn.* 1976, **14**, 2043
9 Johansson, K. E., Palm, T. and Werner, P.-E. *J. Phys. E: Sci. Instrum.* 1980, **13**, 1289
10 Fakirow, S., Fischer, E. W. and Schmidt, G. F. *Macromol. Chem.* 1975, **176**, 2459
11 Werner, P.-E., Eriksson, L. and Westdahl, M. *J. Appl. Cryst.* 1985, **18**, 367
12 Wlochowicz, A. and Przygocki, W. *J. Appl. Polym. Sci.* 1973, **17**, 1197
13 Economy, J., Storm, R. S., Matkovich, V. I., Cottis, S. G. and Novak, B. E. *J. Polym. Sci., Polym. Chem. Edn.* 1976, **14**, 2207
14 Volksen, W., Geiss, R. and Economy, J. *J. Polym. Sci., Polym. Phys. Edn.* 1986, **24**, 2117
15 Hosemann, R. *Z. Physik.* 1950, **128**, 464
16 Lenz, R. W., Jin, J.-I. and Feichtinger, K. A. *Polymer* 1983, **24**, 327
17 Blundell, D. J. *Polymer* 1982, **23**, 359
18 Martin, P. G. and Stupp, S. I. *Polymer* 1987, **28**, 897
19 Blumstein, A. and Thomas, O. *Macromolecules* 1982, **15**, 1264
20 Wunderlich, B. 'Macromolecular Physics: Crystal Nucleation, Growth, Annealing', Vol. 2, Academic Press, New York, 1976